ELSEVIER

Journal of Power Sources 66 (1997) 1–14

JOURNAL OF POWER SOURCES

The role and utilization of pseudocapacitance for energy storage by supercapacitors

B.E. Conway, V. Birss [1], J. Wojtowicz [2]

Chemistry Department, University of Ottawa, Ottawa, Ont., K1N 6N5, Canada

Abstract

The principle of utilizing the non-Faradaic double-layer capacitance of electrode interfaces as a means of storing electrical energy was suggested and utilized in technologies initiated some 37 years ago. However, only over the last ten years has major interest been manifested in commercial development of this possibility in so-called 'supercapacitors' or 'ultracapacitors' based on the large double-layer capacitance achievable at high-area, carbon powder electrodes. In parallel with the utilization of double-layer capacitance is the possibility of use of the large pseudocapacitance that is associated with e.g. electrosorption of H or metal adatoms (underpotential deposition) and especially some redox processes. Such pseudocapacitance arises when, for thermodynamic reasons, the charge q required for progression of an electrode process, e.g. electrosorption or conversion of an oxidized species to a corresponding reduced species in liquid or solid solution, is a continuous function of potential, V; then the derivative dq/dV corresponds to a capacitance but one of a Faradaic kind. This behavior is different from that with an ideal battery where, according to the Nernst equation, V is invariant with state-of-charge measured by q Various experimental examples are shown and characterized, especially that for RuO_2 and other transition metal oxides. Additionally, electroactive polymers such as polyaniline exhibit analogous pseudocapacitative behavior.

Keywords: Supercapacitors; Eenergy storage; Pseudocapacitance

1. Historical remarks

The discovery that electric charges could be stored on the plates of a so-called condenser, now referred to as a capacitor, was made in the mid-eighteenth century during the period when the phenomena associated with 'static electricity' were being revealed. The embodiment known as a condenser is attributed to Musschenbroek [1] in 1746 at Leyden in The Netherlands, whence the name 'Leyden Jar'.

The concept of being able to store, in reasonably small capacitors, relatively large quantities of electrical energy, comparable in magnitude at least with storage energy-densities attainable in batteries, was proposed already some 37 years ago [2]. However, only over the past 10 years or so have such devices [3,4] variously called 'supercapacitors' or 'ultracapacitors, become subject to practical commercial development for the possibility of utilizing them in a hybrid configuration for electric-vehicle power systems and for SLI (starting, lighting and ignition) in regular internal combustion engine (ICE) powered vehicles, as well as for some other smaller scale applications.

An important and fundamental difference between charge storage in a capacitor and that by a battery, is as follows: in the former, actual positive (electron deficiency on one plate) and negative (electron excess on the complementary plate) electrostatic charges physically reside at some two-dimensional charge density, σ, on the plates while a 'charged' electrolytic cell stores charge only indirectly. In the latter case, charges can only be admitted to or withdrawn from the electrodes, from or to an external circuit, when accompanying electrochemical Faradaic processes take place by charge-transfer across an interface, involving changes of oxidation state of the chemical materials of the cell. The two types of processes are distinguished, respectively, by the terms 'non-Faradaic' or 'Faradaic'.

Two principal types of supercapacitor have been investigated, developed and tested: (i) the double-layer capacitor, and (ii) the redox or ad-species pseudocapacitor, the latter being first developed in our laboratory [5,6].

2. Comparison of energy storage in a capacitor and in a battery

The capacitance C of a capacitor is defined by the relation $C = q/V$ where V is the voltage difference between the plates

[1] Present address: Department of Chemistry, University of Calgary, Calgary, Alberta, Canada.

[2] Deceased.

PII S0378-7753(96)02474-3

associated with accommodation of charge q on an area A of each plate. The charge density σ is q/A. If C is not constant with changing V, as often arises in the case of double-layer and pseudo-capacitance at electrodes (see below), a differential capacitance is defined as $C = dq/dV$.

In relation to the geometrical dimensions of a capacitor, C is given by

$C = A\epsilon\epsilon_0/d$ (rationalized system of units)

where d is the separation distance between parallel plates of area A, ϵ is the dielectric constant or relative permittivity of the dielectric material between the plates and ϵ_0 is the permittivity of free-space (8.854×10^{-12} F m^{-1}). From Eq. (1), C is given in F. C per cm^2, for ordinary separation distances (d) of say 0.01 cm, is very small, on the order of pF, even for dielectric materials having $\epsilon \simeq 100$ (for water, $\epsilon = 78$ at 298 K). Large C values are realizable only for very small d and/or very large A (Eq. (1)). That situation is, however, practically attainable by utilizing high specific area powders, e.g. of carbon, for which a double-layer capacitance of $15 - 50$ μF cm^{-2} is associated with the electrode/solution interfaces [7,8] as will be treated later. Such embodiments have been referred to as 'supercapacitors' or 'ultracapacitors', and capacitance densities of tens of F g^{-1} or F cm^{-3} are now attainable.

The energy storable in a charged capacitor is the point of main practical interest with regard to the use of capacitors in the power-source field and for energy transduction. The energy of charging a capacitor or its 'self-energy' (compare the Born self-energy of ions in the gas-phase or in solution [9,10]) is easily calculated as $(1/2)CV^2$ or $(1/2)qV$ for an accumulated charge q residing on plates of a capacitor between which a potential difference of V has been established.

Now in electrochemical charging of a cell exhibiting a Nernstian cell potential (or e.m.f.) of V, V remains ideally constant (practically moderately constant for many battery cell systems except Li-intercalation ones, and quite constant for 95% of discharge in Li/$SOCl_2$ primaries) during charge or discharge until all the reactant materials have been electrochemically consumed, i.e. reduced and oxidized, or vice versa, during discharge or recharge. If the cell charge capacity [3] is Q, the energy stored electrochemically in the cell is QV. For a situation with equal q's ($q \equiv Q$) for a capacitor (q) and a battery cell (Q), charged to the same potential difference, V, between the plates/electrodes, it is seen that the (Gibbs) energies, G, of the charges differ: $G(\text{capacitor}) = (1/2)qV$, while $G(\text{battery}) = QV$, i.e. for given charges and associated voltages, the energy stored in the capacitor is half that for the equivalent battery cell. This arises physically because, in the charging of a capacitor, work has to be continuously done against the charges being accumulated (cf. Ref. [9]) which cause progressively rising voltage in the charging process. In the ideal battery cell, however, the progressively increasing charge, $\int dQ$, is being added at a relatively constant voltage V. Hence $G \simeq QV$.

[3] It is sometimes confusing that the total charge available from a battery in Ah or C is also called 'capacity' of the cell. This is not to be confused with capacitance discussed above, although all battery electrodes also exhibit a significant double-layer capacitance due to their large, real electrochemical interface areas.

3. Distinction between double-layer capacitance and pseudocapacitance

3.1. Double-layer capacitance

In order to place the topic and phenomenon of pseudocapacitance in context in this paper, it will be necessary first to describe the origin and significance of 'double-layer' capacitance against which pseudocapacitance is to be compared and contrasted.

At interfaces between solids and ionic solutions, especially at colloids [11], metal electrodes and semiconductors, a separation of ionic charges, or ionic charges and electronic charges arises, giving rise to the so-called double-layer [7,11–13]. Because an accumulation of charges, Δq, of opposite signs takes place across such interphases to extents dependent on the potential of the electrode (related to the potential difference built up across the interphase, ΔV), a capacitance $C = \Delta q/\Delta V$ or $d(\Delta q)/d(\Delta V)$ arises and is referred to as the 'double-layer' capacitance. It ubiquitously arises at all electrode interfaces and has values typically between about 15 and 50 μF cm^{-2} in aqueous electrolytes [7,8] and less in non-aqueous solvents or in the presence of organic surfactants. The above are large values compared with those attainable per cm^2 in hardware capacitors; the reason is (cf. Eq. (1)) that the charge separation is over only about 3Å in the compact double-layer [7] or up to about 1000 Å over the diffuse part [12,13] of the double-layer. Appreciable C values can, of course, also be attained in electrolytic capacitors where charge separation arises across a thin film of an insulating oxide, several hundred Å's in thickness.

Utilization of the capacitance of the double-layer at electrode interfaces for electrical energy storage is the basis of so-called 'double-layer capacitors' or supercapacitors developed first (in principle) by Becker [2] and by the Sohio group later [14] using high-area carbon powder materials and tetraalkylammonium salt electrolytes.

The potentiality of such systems as vehicles for energy storage arises because large accessible areas per gram are available with various carbon powder materials, typically 100 to 2000 m^2 g^{-1}. Taking an average value [15] of the double-layer capacitance as 25 μF cm^{-2} for carbon (it varies with type and preparation), and a specific real area of say 1000 m^2 g^{-1}, the ideally attainable capacitance density would be 250 F g^{-1}, a very large capacitance! Practically attainable values are in the order of 25 F g^{-1} or less due to limited accessibility of high-area materials to electrolyte and particle

contact limitations. In aqueous media, the practical upper operating voltage is about 1.4 V (determined by the decomposition potential of water, 1.23 V, and other kinetic factors) while in non-aqueous aprotic solvents it can reach 3.5 to 4.0 V. Such high voltage embodiments are, of course, to be preferred as the energy density increases as the square of the voltage on charge. However, non-aqueous electrolytes usually have lower conductivity so power performance can be poorer than with aqueous solutions.

Technologies based on the above principles have led to commercially produced large 'double-layer' capacitors capable of starting internal combustion engine (ICE) vehicles and in hybrid systems with lead/acid or $Zn–Br_2$ batteries for electric-vehicle propulsion where the capacitor functions as a kind of load smoothing device [16].

Charge storage in double-layer capacitance is largely electrostatic in nature (separation of ion and electron charges) and, for this reason, charging/discharging is highly reversible and hundreds of thousands of cycles are typically attainable with a given element of charge being able to be admitted or withdrawn at virtually the same potential. Also, since $C = q/V$ or $V = q/C$, an advantageous direct state-of-charge indication is given by the variation of voltage on charge or discharge, unlike the situation with many (but not all) battery systems. However, in recent years it has come to be recognized that with carbon double-layer capacitors a small but significant 'pseudocapacitance' (see below) can also arise due to some participation of electrochemical surface reactions on the carbon, e.g. reversible surface quinonoid-type redox reactions or chemisorption processes involving partial charge transfer [17–20].

3.2. Equivalent circuit representation

It is convenient to represent the electrical behavior of the electrode interphase in terms of an equivalent circuit, the behavior of which would mimic that of the actual interphase with respect to current or potential responses to modulation, respectively, of potential or current.

The simplest case is that of a double-layer capacitance in series with the solution resistance, R_s (Fig. 1(a)). There is no charge leakage pathway so that such an interphase is referred to as an 'ideally polarizable electrode' [7] which can be realized experimentally to a good approximation at

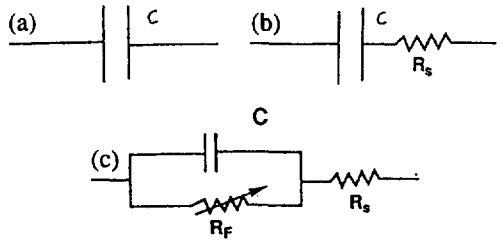

Fig. 1. Equivalent circuits for double-layer capacitance at an electrode-solution interface: (a) ideally polarizable interface; (b) interface with a series resistance, and (c) capacitor with series resistance and potential-dependent Faradaic leakage resistance, R_F.

Hg (+0.23 to −1.0 V RHE, in acid solutions) or Au (−0.1 V to +1.33 V RHE, in alkaline solutions), and to a good extent at C.

In practice, Faradaic leakage currents can arise depending on the electrode potential and solution composition, so circuit (Fig. 1(a)) is modified by inclusion of a Faradaic resistance, R_F, in parallel across C (Fig. 1(c)). R_F is usually inversely related to the electrode potential or overvoltage η according to a Tafel-type equation, in exponential form, viz.

$$i(\eta) = i_0 \exp[-\alpha\eta F/RT] \quad (1)$$

where i_0 is the exchange current-density and α the charge-transfer coefficient. R_F in relation to R_S and C determines the response behavior to changes of V or η, e.g. in pulse of a.c. modulation.

3.3. Significance and origin of pseudocapacitance

In parallel with the development of 'double-layer' capacitors has been the use of so-called 'pseudocapacitance' as a basis for electrical energy storage, initiated in work in this laboratory [5,6] with Continental Group and now continued mainly by Pinnacle Research (Cupertino, CA) and by Giner (Waltham, MA).

The situation required for a pseudocapacitance (designated C_ϕ) to be manifested, i.e. when the potential at which a charge is being passed is a function of the integrated charge accumulated, arises for special thermodynamic reasons. Thus a C_ϕ can be associated with either a redox reaction for which potential is a (log) function of the ratio of activities of the oxidized and reduced species or with a process of progressive occupation of surface sites on an electrode by an underpotential-deposited (UPD) species.

Pseudocapacitance arises in cases where Faradaic charge-transfer processes lead to passage of extents of charge, q, that, for thermodynamic reasons, depend on potential, unlike ideal Nernstian processes where a singular, (ideally) constant electrode potential, e.g. for a metal/metal-ion equilibrium, arises, independent of the extent of the reaction Examples of processes which are associated with pseudocapacitance are as follows:

(i) two-dimensional depositions (so-called underpotential deposition (UPD)) of adatom arrays on electrode surfaces, e.g. H or Cu on Pt, Pb on Au, Bi on Au, Bi on Ag, H on Rh or Pt;

(ii) redox processes in liquid or solid solutions where the electrode potential E (see below) is a function of the log of the ratio of reductant converted to oxidant (or vice-versa) in a redox system, and

(iii) where, in some cases, chemisorption of anions at electrode interfaces takes place with potential-dependent partial Faradaic transfer of an electronic charge [18–20] related to the so-called electrosorption valency [18]. In general, there can be coupling between non-Faradaic double-layer charging and Faradaic surface processes, as discussed in papers by Delahay [19].

Also for Li-intercalation battery systems, e.g. with MoS_2 or TiS_2 cathode materials, the discharging/recharging curves exhibit [21,22] continuously varying potential, V, with state-of-charge, q, so that a pseudocapacitance, $C_\phi = d(\Delta q)/dV$, formally arises.

Each of the above types of process leads to an experimentally accessible capacitance, C_ϕ, which is, however, usually potential-dependent [23]. It is to be noted, in contrast to the case of an ideal double-layer capacitance, that charging and discharging of a pseudocapacitor takes place through Faradaic processes involving electron transfer across the electrode/solution interface. Since, however, such a process necessarily takes place at such an interface, an additional (usually much smaller) double-layer capacitance also arises in some parallel coupling with the C_ϕ (see equivalent circuit below), and is non-Faradaically charged with changing potential.

3.4. Equivalent-circuit representation involving C_ϕ

As with the representation of double-layer charging behavior, an equivalent circuit representation can be given for charging of a pseudocapacitance C_ϕ through a Faradaic resistance R_F and some possible further Faradaic resistance R_D for discharge (e.g. desorption of an ad-species). This combination (see Fig. 2) involves a Faradaic impedance (C_ϕ, R_F and R_D) in parallel with C_{dl}. Usually, over a certain range of potentials, C_ϕ can be $\gg C_{dl}$.

For practical high-area, porous electrode structures, at which large C_{dl} or C_ϕ values are developed, the equivalent circuit is much more complex than those in Fig. 1(a) and (c) or Fig. 2 due to an effective distributed series/parallel arrangement (Fig. 3) of the components of the impedance Z. Then the circuit has a wide range of relaxation frequencies (ω) for a.c., or time domains (τ) for pulse modulations, e.g. pulse discharging and recharging. This is practically a very important aspect of the properties of high-area, porous C_{dl} or C_ϕ supercapacitors and determines their power performance on discharge or their power spectrum as $f(\omega$ or $\tau)$.

A model illustration of the complexity of the equivalent circuit for a porous capacitor electrode is shown in Fig. 3. The capacitative or Faradaic impedance elements can be C_{dl}, or C_ϕ and C_{dl}, each as represented by Fig. 1(b) or Fig. 2. Also shown is a Faradaic leakage resistance across each capacitance element that may or may not be practically significant depending on conditions.

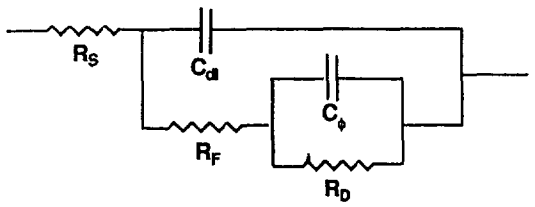

Fig. 2. Equivalent circuit for an electrode interface exhibiting Faradaic pseudocapacitance C_ϕ in a parallel relation, through an R_F, with the double-layer capacitance, C_{dl}.

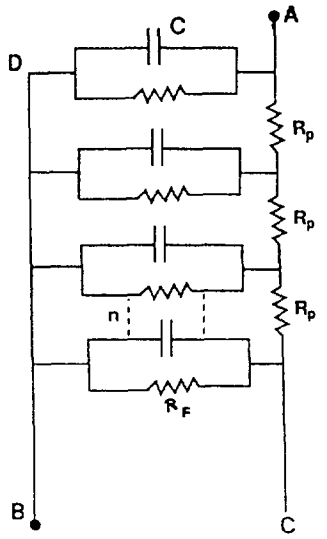

Fig. 3. Complex equivalent circuit (schematic) for a porous electrode with distributed capacitance, and solution and matrix resistances.

4. Adsorption and redox pseudocapacitance as a basis for supercapacitors

As explained above, a very different basis for development of supercapacitors arises from utilization of pseudocapacitance. Such systems provide a transition case between double-layer electrostatic charge storage and electrochemical battery-cell charge and energy storage. As indicated in the previous section, two types of pseudocapacitance can arise in electrochemical processes: (i) adsorption pseudocapacitance, and (ii) redox pseudocapacitance; we consider each in more detail as follows; both usually meet the requirement of good reversibility, characteristic of capacitance behavior.

4.1. Adsorption pseudocapacitance

Two-dimensional surface reactions give the best example of reversible processes associated with so-called adsorption pseudocapacitance which can be 10–100× greater than the double-layer capacitance at the same electrode. Faradaic deposition and desorption of H (coverage θ) at Pt, Rh or Ir are useful examples to consider. The surface reaction equation is, for the example of Pt in acidic solutions:

$$\underset{1-\theta_H}{Pt} + \underset{C}{H_3O^+} + \underset{V}{e^-} \overset{k_1}{\underset{k_{-1}}{\rightleftarrows}} \underset{\theta_H}{Pt\,H_{ads}} + H_2O \qquad (2)$$

free surface site fraction; potential; occupied surface site fraction

For an equilibrium situation at any potential it can be shown in a well known way that

$$\frac{\theta_H}{1-\theta_H} = \frac{k_1 C_{H_3O^+}}{k_{-1}} \exp(-VF/RT) \qquad (3)$$

(V is negative for the cathodic direction of current) or, explicitly for θ_H,

$$\theta_H = \frac{K_1 C_{H_3O^+} \exp(-VF/RT)}{1 + K_1 C_{H_3O^+} \exp(-VR/RT)} \quad (4)$$

where K_1 $(=k_1/k_{-1})$ is an electrochemical equilibrium constant for H chemisorption with charge transfer (Eq. (2)). Eq. (4) shows that the coverage by H is a continuous function of V from $\theta_H = 0$ to $\theta_H \rightarrow 1$ and, for the equilibrium situation, V is an equilibrium potential corresponding to each and any value of θ_H in the above range. The dependence of θ_H on V is shown in Fig. 4 and is effectively a two-dimensional charging curve for H on the surface. Eq. (4) corresponds to an electrochemical Langmuir isotherm for electrosorption of H. However, in practice, even at single-crystal surfaces of Pt, progressive adsorption of H from $\theta_H = 0$ to $\theta_H \rightarrow 1$ occurs in several distinguishable stages.

Of special significance for supercapacitance discussed in this paper, is the result of differentiating Eq. (4) which gives then a quantity having the significance of a pseudocapacitance $C_\phi = Q_1(d\theta_H/dV)$ where Q_1 is the Faradaic charge required for deposition of desorption of a monolayer of H ($Q_1 \cong 210\ \mu C\ cm^{-2}$ for 1 atom of H per Pt atom in the surface ($\theta_H \rightarrow 1$) — this Q_1 depends a little on the orientation of surface planes exposed). From Eq. (4), the result is

$$\left(\frac{RT}{F}\right)\frac{C_\phi}{Q_1} = \frac{K_1 C_{H_3O^+} \exp(-VF/RT)}{1 + K_1 C_{H_3O^+} \exp(-VF/RT)^2} \quad (5)$$

which is plotted as $f(V)$ also in Fig. 4. For a single-state process, it has a large maximum value of $\sim 2200\ \mu F\ cm^{-2}$, i.e. about 100 times the double-layer capacitance. For multistate adsorption, the value is diminished 5–10 times but extends over a wider potential range (see Fig. 4). C_ϕ is referred to as a 'pseudo'-capacitance (cf. Ref. [23]) since it arises from Faradaic charge-transfer reactions and not from electrostatic charging that is the origin of double-layer capacitance.

It is important to note that the behavior of the process [2] according to Eq. (5) and experiment is (i) highly reversible with respect to changes of dV/dt (e.g. in cyclic voltammetry) from negative to positive values, i.e. 'mirror-image' curves of C_ϕ versus V arise; (ii) the C_ϕ versus V profile is repeatable over many thousands of cycles in a clean solution, and (iii) that this reversibility is maintained up to quite high sweep rates of $\sim 100\ V\ s^{-1}$. Similar behavior is observed [26] for other two-dimensional electrode processes, e.g. reversible deposition and desorption of Pb and Bi adatoms on Au or Ag over a 0.6 V range. This is because only two-dimensional array structures are involved without any three-dimensional phase changes or reconstructions of the type that arise in charging of bulk battery materials and can be irreversible. These properties, determined by Eqs. (4) and (5), are the basis of supercapacitor operation depending on pseudocapacitance of two-dimensional films.

In the case of chemisorption in UPD processes, the relation of potential to coverage usually follows an isotherm (cf. Eq. (3)) of the form

$$(\theta/1-\theta) = K_1 \exp(-g\theta)\ C \exp(VF/RT) \quad (6)$$

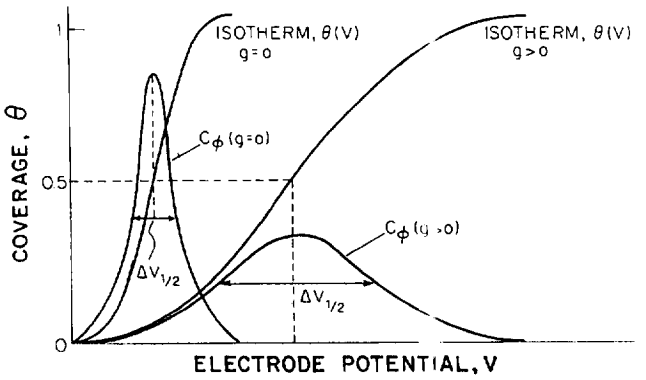

Fig. 4. Relation of potential dependence of C_ϕ to potential dependence of coverage, θ, of an electroactive species adsorbed at an electrode surface.

where g is a parameter characterizing the θ-dependent Gibbs energy of lateral interactions between the adsorbate particles [23]. For $g = 0$, Eq. (6) is an electrochemical Langmuir isotherm like Eq. (3). Noting that charge has to be passed to produce changes of θ (Eq. (2)) requiring charge Q_1 for completion of a monolayer ($Q_1 \simeq 210\ \mu C\ cm^{-2}$ for H on Pt), differentiation of Eq. (6) leads to pseudocapacitance C_ϕ as in Eq. (5).

The adsorption isotherm (charging curve for UPD species) and its differential (giving C_ϕ) are plotted in Fig. 4 for $g = 0$ and $g = 5$. When $g > 0$, C_ϕ is less than its value for $g = 0$ but it retains appreciable values over a wider potential range [23]. For $g = 0$, C_ϕ has a large maximum of about 2200 $\mu F\ cm^{-2}$.

Since the processes of charging or discharging of a pseudocapacitance (e.g. as in Eq. (2)) involve passage of Faradaic charge, kinetic limitations can arise depending on the respective rate constants of the processes or the corresponding Faradaic resistance (Fig. 2). The kinetic behavior of such surface processes, as exhibited in cyclic voltammetry conducted over a range of sweep rates, was treated by Srinivason and Gileadi [27] and by Kozlowska et al. [28].

The rates of the forward and backward directions of the (single-state) surface process (e.g. for process (2)) are written as:

$$\vec{i} = Fk_1 C(1-\theta_H) \exp -\beta F(V \pm st)/RT \quad (7)$$

$$\overleftarrow{i} = Fk_{-1}\ \theta_H \exp(1-\beta)F(V \pm st)/RT \quad (8)$$

and net currents as $\vec{i} - \overleftarrow{i}$. The potential V is modulated in time t by the potential sweep rate s ($V(t) = V(t=0) \pm st$ in the sweep). θ_H is then a $f(V,t)$ in a linear-sweep voltammetry experiment.

We have used such equations to illustrate the onset of kinetic irreversibility in a surface process exhibiting pseudocapacitance, as s is increased. The effect of such increase of s is conveniently represented in terms of plots for various values of reduced sweep rate, s/k, as shown in Fig. 5. For increasing s/k, the anodic and cathodic current-response profiles (Fig. 5) become increasingly displaced from one another in the mirror-image relation for reversible behavior, and thus become asymmetric [27].

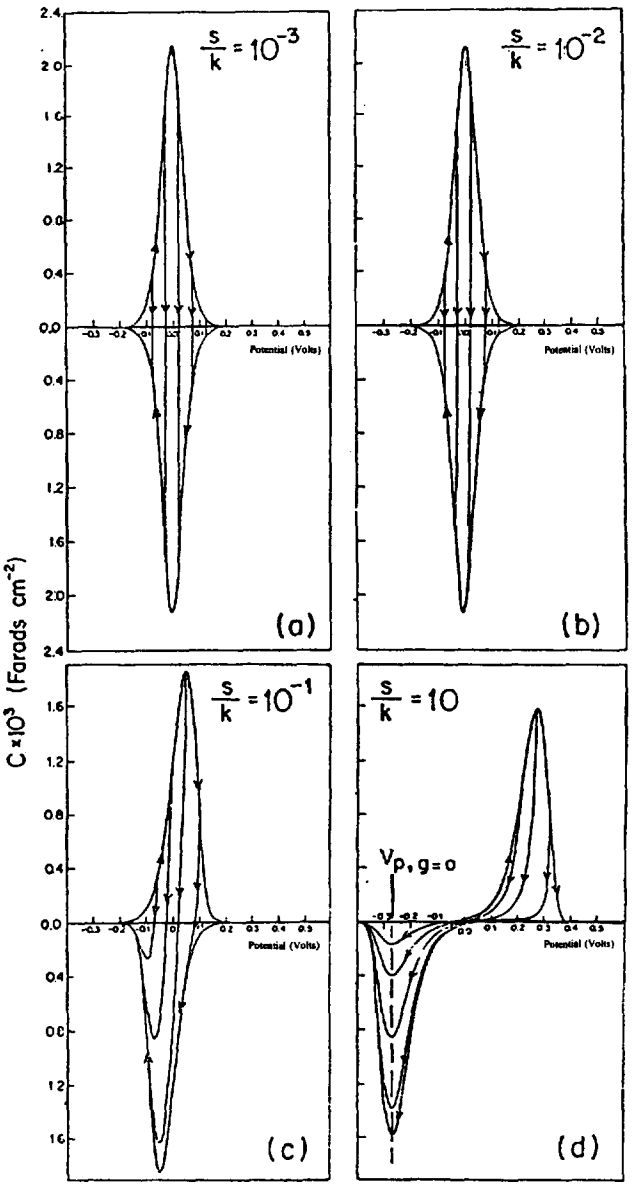

Fig. 5. Changes of reversibility of a surface charging process with increase of sweep rate (s) in cyclic voltammetry expressed in terms of the rate constant k of the process expressed as a reduced sweep-rate parameter, s/k.

The behavior illustrated in Fig. 5 is very important practically as the onset of irreversibility causes diminution of reversibly accessed charge and also to power losses. The irreversibility corresponds to significant overvoltages being required to conduct the surface processes at appreciable rates which must arise at larger s values (note $i = Cs$, see Eq. (11)).

4.2. Redox pseudocapacitance

The potential of a redox system, $ox + ze^- \rightleftharpoons red$, is given by the Nernst equation

$$E = E^0 + \frac{RT}{zF} \ln [ox] / [red] \equiv E^0 + \frac{RT}{zF} \ln \frac{[ox] / [red]}{1 - [ox] / [red]} \quad (9)$$

Since the concentrations (or activities) of 'ox' or 'red' can be expressed as relative fractions $[ox]/([ox]+[red])$ and $[red]/([ox]+[red])$, so that the latter is $1-[ox]/([ox]+[red])$, then $\ln [ox]/[red] \equiv \ln (\Re/1-\Re)$ where $\Re$ is defined as $[ox]/([ox]+[red])$.

It is seen that the above factor in $\Re/(1-\Re)$ is formally analogous to that, $(\theta_H/1-\theta_H)$, for electrochemical adsorption with charge transfer, in terms of coverage fraction θ (Eq. (3) in log form) that gives rise to the adsorption pseudocapacitance C_ϕ, for coverage θ, analogous to $[red]/([red]+[ox])$ in Eq. (9). Thus a redox capacitance is formally analogous to an adsorption capacitance with charge transfer. Since a charge Q ($=zF$) is required to convert a given quantity (1 mole) of 'ox' to 'red' (or vice versa), differentiation of Eq. (9) gives rise to a pseudocapacitance (Table 1) having the same relation to potential as the C_ϕ of Eq. (5). Similar behavior arises for lithium intercalation into layer-structure materials [21]. The electrochemical thermodynamic relations for the three cases, adsorption, redox and three-dimensional intercalation, are compared in Table 1.

Practically, a redox capacitance can involve diffusion control if both 'Ox' and 'Red' are solution species. However, this complication can be avoided by physically or chemically anchoring the redox species on a polymer at the electrode surface or using an electro-active polymer [6,24]. Since the charge Q is determined by the total concentration $[ox]+[red]$ which can be quite large (e.g. for 1 M solution of a $z=1$ system, $Q = 96.5$ C cm^{-3}, the C_ϕ can be very large but only over a restricted potential range, ~120 mV.

Table 1
Correlation of types systems giving rise to pseudocapacitance with application to supercapacitors

System type	Essential thermodynamic relations
(a) *Redox system*	$E = E_0 + (RT/zF) \ln \Re/(1-\Re)$
$Ox + ze^- \rightleftharpoons$ Red and $O^{2-} + H^+ \rightleftarrows OH^-$ in oxide lattice	$\Re = [Ox]/([ox]+[Red])$; $\Re/(1-\Re) \equiv [Ox]/[Red]$
(b) *Underpotential deposition*	$E = E_0 + (RT/zF) \ln \theta/(1-\theta)$
$M^{z+} + S + ze^- \rightleftharpoons S \times M$	
($S \equiv$ surface lattice sites)	$\theta =$ 2-dimensional site occupancy fraction
(c) *Intercalation system*	$E = E_0 + (RT/zF) \ln X/(1-X)$
Li^+ into 'MA_2'	$X =$ occupancy fraction of layer-lattice sites (e.g. for Li^+ in TiS_2)

Note: (b) and (c) can be regarded as mixing of occupied (X or θ) sites with unoccupied sites, $(1-\theta)$ or $(1-X)$. Hence the analogy to [red] and [ox].

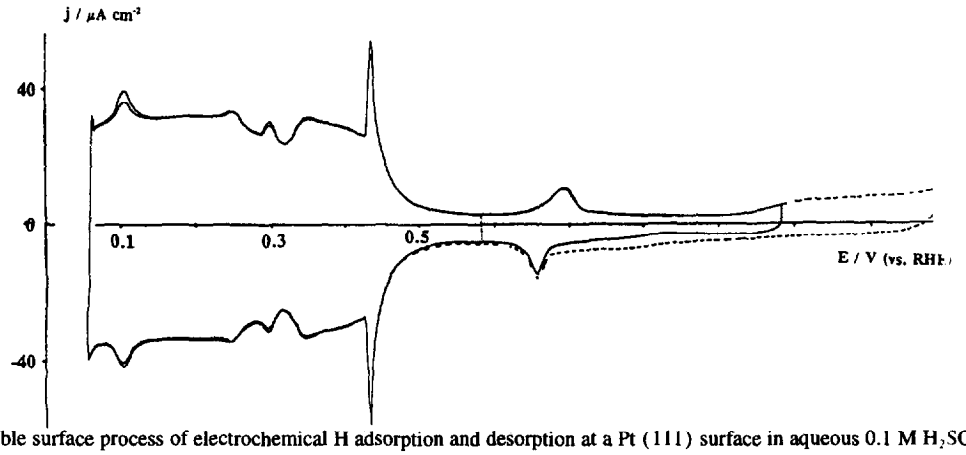

Fig. 6. Highly reversible surface process of electrochemical H adsorption and desorption at a Pt (111) surface in aqueous 0.1 M H_2SO_4 (298 K), illustrated by the 'mirror-image' cyclic voltammogram. (The anodic and cathodic currents correspond to the H adsorption pseudocapacitance, $C_\phi = i/s$.) Pt (111) flame-treated electrode after cooling in air, and sweep rate = 50 mV s^{-1}.

4.3. Lithium intercalation electrodes — a transitional behavior

An important transitional behavior between supercapacitors and batteries arises with processes involving Li^+ intercalation into layer-lattice host cathode materials, e.g. MoS_2, TiS_2, V_6O_{13}, CoO_2, etc. Normally these cathode materials, coupled with an Li anode or an Li/C anode, would be regarded as 'battery' cathode materials. However, the forms of the charge/discharge curves (equations in section (c) in Table 1) and associated pseudocapacitance, and even the cyclic voltammetry profiles, are similar to those for two-dimensional electrosorption (UPD), as illustrated in Fig. 6(a) and (b).

The thermodynamics of sorption of Li into layer-lattice intercalation host materials have been worked out by Haering and MacKinnon [21] in terms of three-dimensional lattice statistics which lead to three-dimensional sorption isotherms, in site-fraction X, having similar forms to that of Eq. (6). Thus, such systems exemplify a transition between supercapacitor and battery behavior.

The essential and common thermodynamic feature of systems that can give rise to pseudocapacitive behavior is thus the relation of free energy to the log of the configurational activity terms, $\theta/(1-\theta)$ for two-dimensional adsorption, of $X/(1-X)$ for three-dimensional sorption and $[ox]/[red]/(1-[ox]/[red])$ for redox processes as summarized in Table 1.

5. Electrical response functions for capacitors

The characteristics of capacitative charging behavior can be usefully manifested and practically evaluated by the several types of electrical response functions that arise when various types of signal are addressed to the capacitor, e.g. a d.c., potential step, current pulse or a.c., as follows:

(i) In a charging curve at constant current, i, the potential difference, ΔV, across the capacitor plates changes linearly with time; with the definition $C = \Delta q/\Delta V$ and with $\Delta q = \int i\,dt$, then

$$C = \int i\,dt/\Delta V = i\,\Delta t/\Delta V \tag{10}$$

(ii) In a cyclic-voltammetry experiment at a voltage sweep rate $s = dV/dt$ (= constant), a capacitative charging current, i, arises

$$i = C(dV/dt) = Cs \text{ or } C = i/s \tag{11}$$

In a sweep-reversal experiment at constant $\pm s$, the current response profile is ideally a rectangle along the time–potential axis when C is constant or, if it is not, then a differential profile of C is generated often with peaked structure. The direction of current is immediately reversed upon reversal of direction of the potential sweep for a purely capacitative process. This is not, however, necessarily the case if there is any kinetically slow process involved, e.g. in the case of charging a pseudocapacitance through an appreciable R_F (Fig. 2).

(iii) In a discharge experiment through a load resistance, R, the time-dependence of potential is

$$V(t) = V_0 \exp[-t/RC] \tag{12}$$

Hence the slope of a log $V(t)$–t plot has value $-1/RC$, the inverse time constant of the circuit containing the capacitance element.

(iv) In the case of self-discharge through a Faradaic leakage process, the load resistance is effectively a potential-dependent Faradaic resistance related to the Tafel equation for the leakage process. In this case (for the exponential form of the Tafel relation)

$$-C\,dV/dt = i_0 \exp(\alpha VF/RT) \tag{13}$$

which, after rearrangement to $\exp(-\alpha VF/RT)\ dV = -i_0 C\,dt$, integrates to

$$-RT/\alpha F \exp(-\alpha VF/RT) = -i_0 Ct + \tau \tag{14}$$

giving $-V(t) \propto \ln(t - \tau/i_0 C)$ where τ is an integration constant. Self-discharge is a practically important aspect of

supercapacitor behavior where a Faradaic leakage process can arise, e.g. due to a redox shuttle reaction between the electrodes because of impurities or the presence of O_2. The slope, from Eq. (14), of the $-V(t)$ versus $\log t$ self-discharge transient can be useful for characterizing the origin of the leakage current.

(v) In an a.c. impedance experiment, the (imaginary) component of impedance is $Z'' = 1/j\omega C \equiv -j/\omega C$ and ideally the real component Z', is infinity. In practice, this is rarely the case, e.g. as for Fig. 3.

6. Experimental characterization of pseudocapacitance

Here we show results for several types of systems in which appreciable or large values of C_ϕ per cm^2 are experimentally realizable. Only a few systems are, however, practically applicable to supercapacitors.

6.1. Adsorption pseudocapacitance

The first examples that were considered [5,6] were based on the very reversible behavior of H underpotential deposited (UPD) at Pt [25], illustrated in Fig. 6 from aqueous acid or alkaline solutions. The behavior deviates from that for simple Langmuir chemisorption (Eq. (3)) since several current-response peaks, rather than a single one, are observed, even on a single-crystal surface (Fig. 6). The latter phenomenon arises because in formation of a monolayer of H several array configurations arise, with transitions between them, before a complete monolayer (1 H per Pt atom, $\equiv \sim 210\ \mu C\ cm^{-2}$). The average pseudocapacitance realized is about 400 $\mu F\ cm^{-2}$ (for a single peak it would be $\sim 2200\ \mu F\ cm^{-2}$). Although the H pseudocapacitance on Pt behaves very reversibly in a capacitative manner, the cost of the substrate material is large and the useable voltage range is only 0.35 V.

Another interesting example is the UPD of Pb on Au; again several pseudocapacitance charging-peaks arise in cyclic voltammetry, even on single-crystals [26]. The voltage range for realization of appreciable pseudocapacitance is ~0.6 V in this case. Again the substrate material is expensive but Ag is a cheaper alternative.

6.2. Transitional behavior with lithium intercalation

Fig. 7(a) shows an example of the sorption (discharging) isotherm as a function of lattice site occupancy, X, for a three-dimensional intercalation process, e.g., for Li into TiS_2 [21]. Since Faradaic charge is required for deposition of, e.g., Li into an intercalation host, X depends continuously on charge passed. The relation of V to X can be differentiated, as for Eq. (3), so that formally a pseudocapacitance arises (as in Eq. (5)) as illustrated in Fig. 7(b). The similarity of intercalation behavior to two-dimensional chemisorption (UPD) arises because the sorption of Li into a layer-lattice host is, in fact, closely similar to two-dimensional adsorption: the Li ions are actually accommodated in quasi-two-dimensional planes in the van der Waals gap of the host lattice material.

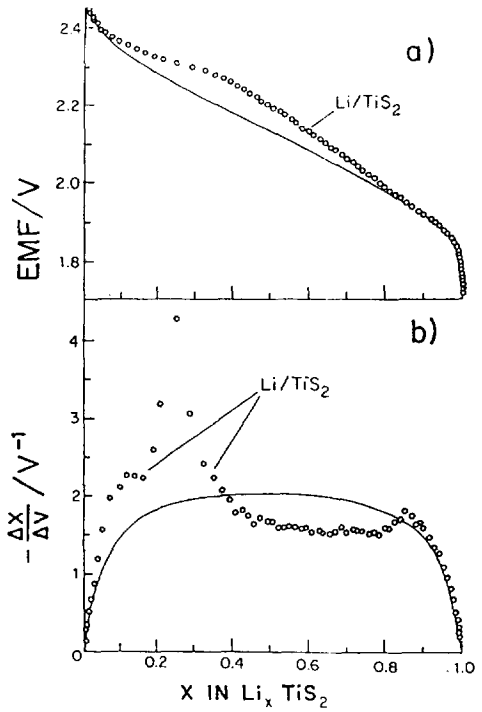

Fig. 7. (a) Discharge curve (sorption isotherm for Li^+ intercalation) for an Li/TiS_2 battery electrode system associated with intercalation of Li^+ (from Ref. [21]). (b) Differential curve of the data of Fig. 7(a), corresponding to manifestation of a pseudocapacitance (from Ref. [21]).

6.3. Redox pseudocapacitance

Here the first experimentally characterized example [6] is that of ferrocyanide bound in a polyvinylpyridine film at a gold substrate electrode (Fig. 8), to minimize diffusion effects. A good reversible response is observed and the system can be cycled many times. The situation for a diffusing redox species is exemplified by the asymmetric curves in Fig. 9.

The second example, on which much more work has been carried out, is the Ru/RuO_2 electrode. RuO_2 can be either grown in a hydrous oxide state by cycling Ru metal between 0.0 and 1.4 V, RHE many times (> 1000 cycles) or prepared by thermal decomposition of $RuCl_3$ or $(NH_4)_3RuCl_6$. The RuO_2 films thus formed are easily visible under scanning electron microscopy (Fig. 10) and have thicknesses up to several μm. The oxide film thus developed exhibits a remarkably reversible cyclic voltammogram (Fig. 11) that is not degraded over many thousands of cycles. Also, it approaches the ideal 'rectangular' form (Fig. 10) characteristic of a capacitance that is independent of potential. The operating charge/discharge voltage range is 0.05 to 1.4 V before either H_2 or O_2 evolution impairs the capacitative behavior.

It is believed that the capacitative behavior arises on account of several overlapping redox processes involving proton and electron injection (or removal) that remain highly reversible because no phase changes arise. The material is an

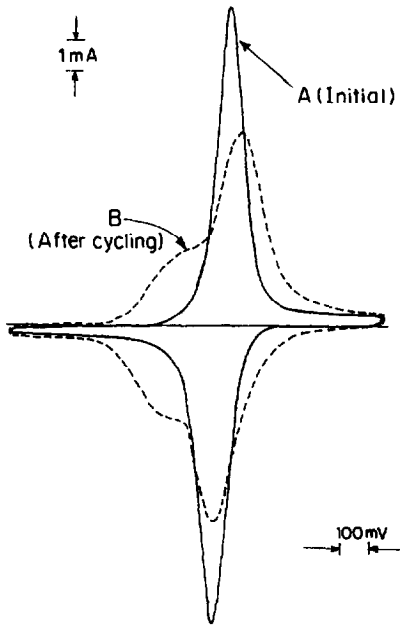

Fig. 8. Reversible redox pseudocapacitance developed with $[Fe(CN)_6]^{3-}$ / $[Fe(CN)_6]^{4-}$ bound on a polyvinylpyridine polymer attached to a gold electrode interface. Redistribution of charge, sulfate system, pH = 1.09. (———) 60 min of cycling (180 cycles) in $[Fe(CN)_6]^{-3}$, and (- - -) 19 h of cycling (3400 cycles) in $[Fe(CN)_6]^{-3}$.

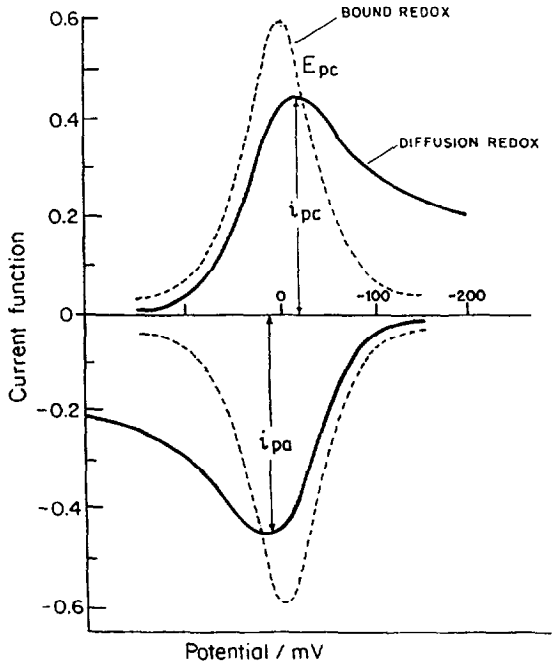

Fig. 9. As in Fig. 8 but when diffusion processes involving the redox reactants are involved: (a) redox pseudocapacitance for an anchored (surface-bound) redox species, and (b) for a redox reaction under diffusion-controlled process at an electrode interface.

hydrous oxide having a porous structure, so a significant double-layer capacitance component is also present, probably 10–15% of the total $C_{dl} + C_{\phi}$.

The response of the RuO_2 system is typical, on d.c. discharging, of a true capacitance, Fig. 12 shows a normalized

Fig. 10. Scanning electron microscopy picture of hydrous-oxide film of RuO_2 developed by anodic cycling of Ru metal 1 M in aq. H_2SO_4. Film thickness about 5 μm.

plot of d.c. discharge behavior of RuO_2 in 1 M H_2SO_4 into load resistances R having various values from 100 kΩ to 63Ω. The experimental points in Fig. 12 fall on a common curve indicating constancy of capacitance under these 'd.c.' conditions. The form of the plot derives from Eq. (12), i.e. $V(t) = \exp(-t/RC) + \text{constant}$ and $V(t) = i(t)R$, the time-dependent potential difference across C. t/RC is a reduced time, scaled by the time constant, RC.

It is seen that, from many potentials along the potential-scan range (Fig. 11), the sweep direction can be reversed giving an almost immediate reversal of direction of response current. This is also a characteristic of capacitor behavior. Any kinetic limitations give rise to a delay in the response to sweep reversal as illustrated by the theoretical curves in Fig. 5.

The behavior under a.c. modulation exhibits a major dispersion of capacitance (Fig. 13) which is typical of porous electrode behavior (cf. equivalent circuit, Fig. 3). RuO_2 can also be dispersed as a film, thermally formed on glass [29], glass particles or carbon. The behavior is very similar to that of the film on metallic Ru (Fig. 11).

Experiments were also conducted with other elements, Mo, W and Co, to examine if corresponding redox pseudocapacitance behavior could be generated at such cheaper metals. Anodic/cathodic cycling at these metals also produces hydrous oxide films exhibiting almost mirror-image cyclic voltammograms (Figs. 14 and 15) but with less constancy of redox C_{ϕ} with potential. The potential ranges of useful C_{ϕ} values are also smaller, e.g. 0.8 V.

As was pointed out in Ref. [5], electro-active polymers, e.g. polyaniline, also exhibit reversible charge/discharge behavior in cyclic voltammetry with a potential range of ~0.7 V. Again the electrical behavior arises from redox processes involving production or consumption of charges electrochemically generated on the polymer chains. Fig. 16 shows the reversible cyclic voltammetry behavior of polyaniline in aqueous H_2SO_4. Other electro-active polymers, e.g.

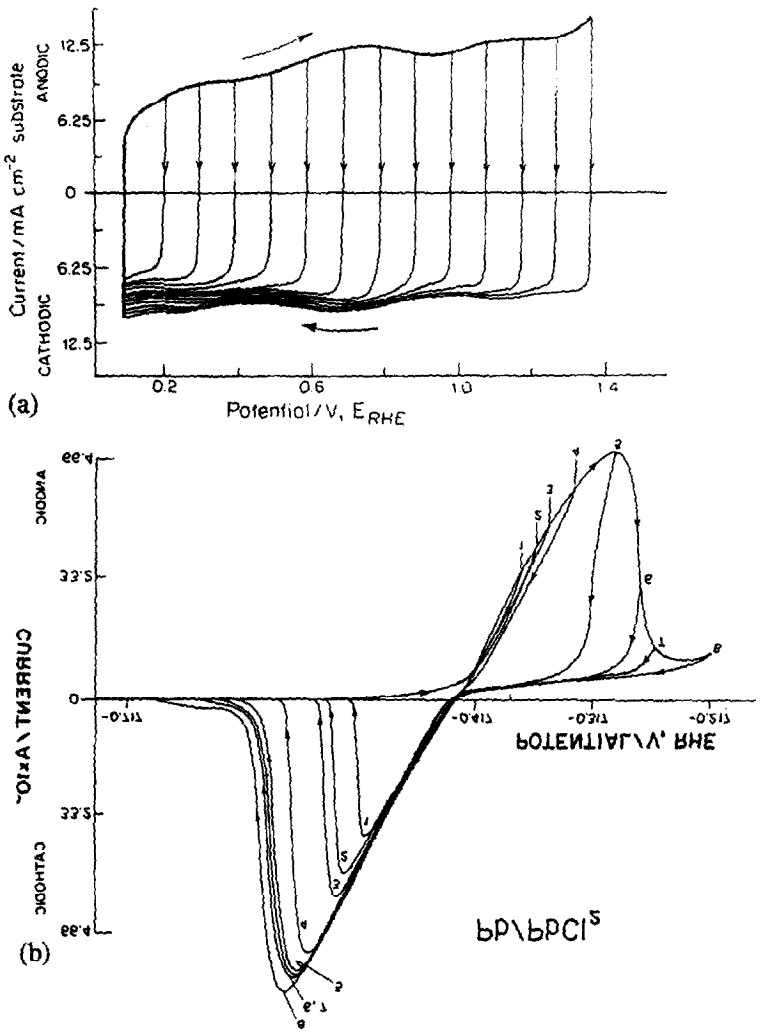

Fig. 11. (a) Reversible, 'mirror-image' cycling voltammogram for an RuO_2 film in aq. H_2SO_4 illustrating manifestation of a (solid-state) redox pseudocapacitance. Diagram also shows successive changes of sweep direction made at various potentials between 0.05 and 1.4 V RHE. (b) Non-mirror image curves for cyclic voltammetry of a battery-type process, $Pb + 2Cl^- \rightleftharpoons PbCl_2 + 2e^-$.

polythiophene, exhibit similar or better behavior as demonstrated by Rudge et al. [24].

'Mirror-image' relations between anodic and cathode current-response profiles in cyclic voltammetry are an important characteristic of reversible pseudocapacitance charge/discharge processes. By contrast, battery charge/discharge processes are usually entirely irreversible, in this sense, i.e. the anodic and cathodic current profiles are not mirror images. This is exemplified for the process $Pb + 2Cl^- \rightarrow PbCl_2$ (solid) $+ 2e^-$, a battery-type reaction, in Fig. 11(b) (contrast Fig. 11(a)). Similar behavior occurs with $PbSO_4$ formation at Pb or CdO at Cd. This difference arises because such processes involve significant overpotentials, one side or the other of the reversible potential, and phase changes. Also, the thermodynamic state of the reagent and product remain almost constant with extent of formation or reduction of the product, e.g. $PbCl_2$ and $PbSO_4$. With UPD behavior [23,28] or some redox reactions (Figs. 8 and 9), the systems exhibit a thermodynamic potential that is a continuous function of extent of charge measured by $\theta/(1-\theta)$ or $\Re/(1-\Re)$ as in Table 1, giving rise to a C_ϕ.

7. Experimental distinction between double-layer and pseudocapacitance

A problem of current significant interest is how the double-layer capacitance at an electrode interface can be distinguished (cf. Ref. [19]) from any appreciable pseudocapacitance that may arise, e.g. for H chemisorption or redox processes at RuO_2 capacitor electrodes. It has recently become recognized that at porous carbon surfaces at which nominally double-layer capacitance principally arises, nevertheless significant pseudocapacitance may also be manifested. This can be due to anion chemisorption with partial charge transfer [17–20] or due to redox processes, e.g. involving quinonoid functional groups at the carbon interface.

A pure capacitance is ideally polarizable, i.e. no leakage currents pass on open circuit. The double-layer at Hg electrode almost behaves in this way from +0.2 to −1.0 V (RHE) as does the double-layer at an Au electrode from −0.1 to +1.3 V (RHE). Beyond these limits, Faradaic cur-

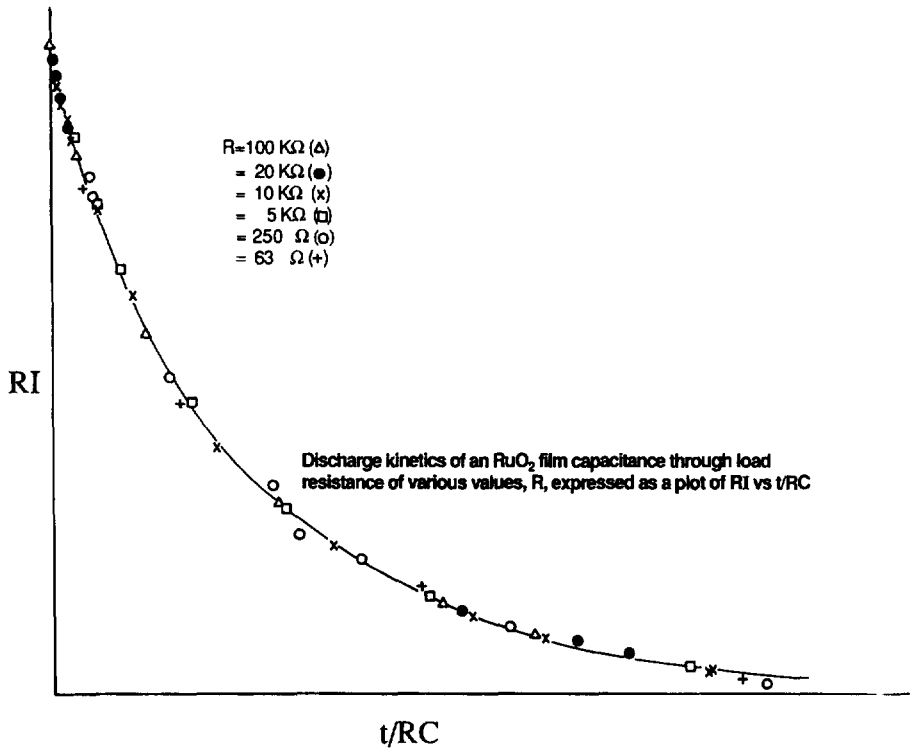

Fig. 12. Normalized common curve for d.c. discharges of a charged RuO_2 electrode in 1 M H_2SO_4 into load resistances, R, having a wide range of values.

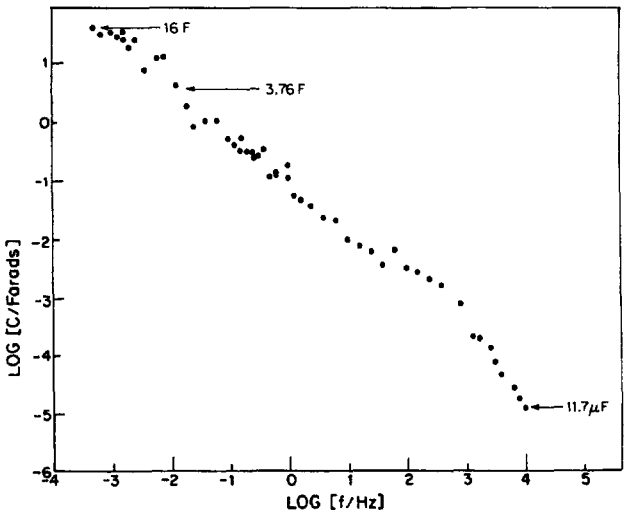

Fig. 13. Dispersion of pseudocapacitance of an RuO_2 film with increasing frequency in an a.c. impedance experiment.

rents pass due either to decomposition of the solution or to oxidation of the electrode material.

Contrarily, a pseudocapacitance, as represented in Fig. 2, requires passage of Faradaic charge in order for its potential to be changed, i.e. electrochemical processes such as redox reactions or H electrodeposition, take place.

Practically, an experimental distinction can usually be made between charging (or discharging) processes involving the double-layer capacitance (C_{dl}) and a pseudocapacitance (C_ϕ); it is based on the different orders of relaxation time constants RC that are exhibited by the double-layer capacitance and a pseudocapacitance. Because C_{dl} is usually of the order of 20–50 μF cm^{-2} while C_ϕ is of the order of 500–1000 μF cm^{-2} (but sometimes dependent on potential, e.g. for H or metal adatom electrosorption [23,26–28]) the RC time constant for charging C_{dl} (when solution resistance is not small, i.e. for electrolyte concentration >0.1 M) is usually 10–100 times smaller than that for C_ϕ. C_ϕ is also coupled with the potential-dependent Faradaic resistance, R_F in Fig. 2. Note that when R_F is not negligible, as is usually the case, C_{dl} and C_ϕ are not coupled in a simple parallel way, i.e. giving additivity of their values. If that were the case they could not be experimentally distinguished, e.g. in an a.c. impedance measurement.

When the RC time constants are different, as indicated above, then it is possible unambiguously to distinguish C_{dl} from C_ϕ by determining the impedance spectrum of the electrode interface over a wide range of frequencies, e.g. from 0.01 Hz to say 100 kHz, and plotting the resolved real (Z') and imaginary (Z'') components of impedance (Z) in the complex-plane for the range of frequencies, ω, covered in the experiment. Then two separate semicircles relating the Z'', Z' components arise: the one in the high-frequency region corresponds to modulation of the C_{dl} charge and that over the low-frequency region to modulation of the charge held by C_ϕ. Complications may arise, however, when the equivalent circuit approaches that shown in Fig. 3, e.g. for a porous electrode at which a distribution of RC time constants can be involved. For the case where a capacitor electrode is overcharged, i.e. solution decomposition Faradaic processes take place, we have recently developed a procedure [31] for quan-

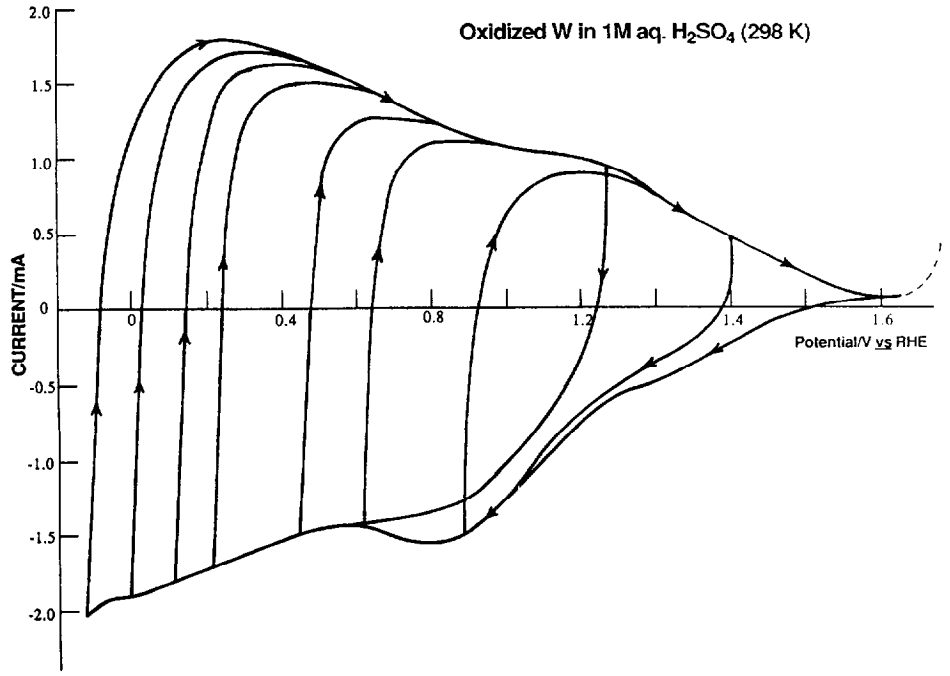

Fig. 14. Development of 'mirror-image' cyclic voltammogram for an oxide film formed on W by potential cycling in aq. H_2SO_4.

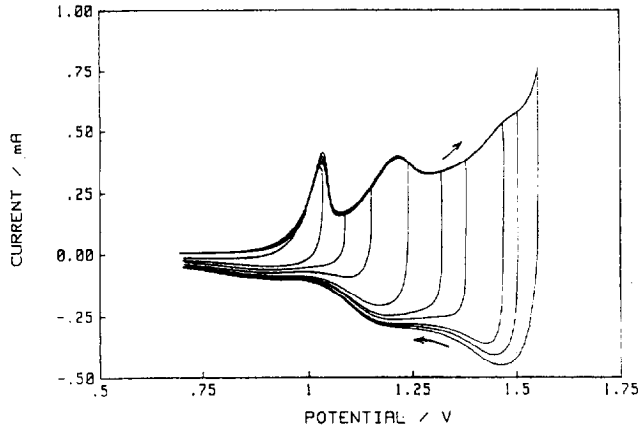

Fig. 15. As in Fig. 14 but for Co in 1 M aq. KOH.

titative analysis of potential-relaxation transients (at a Pt electrode).

The essential basis of the potential-relaxation procedure is that when a Faradaic overchange current is interrupted, charge continues to pass across the double-layer by the same process as that which was previously taking place prior to the interruption, i.e. C_{dl} is then in a non-ideally-polarizable condition, represented actually by Fig. 1(c), and Eq. (15) applies.

When a C_ϕ, as well as the ubiquitous C_{dl}, is significant, both C_{dl} and C_ϕ become discharged on open circuit but because they usually have widely different C and hence RC values, their response in the time-domain transients is usually distinguishable.

The basic relation for the initial potential relaxation rate at the moment of current interruption (time $t=0$) is

$$i(t=0) = -C_{dl}(dV/dt)_{t=0} \quad (15)$$

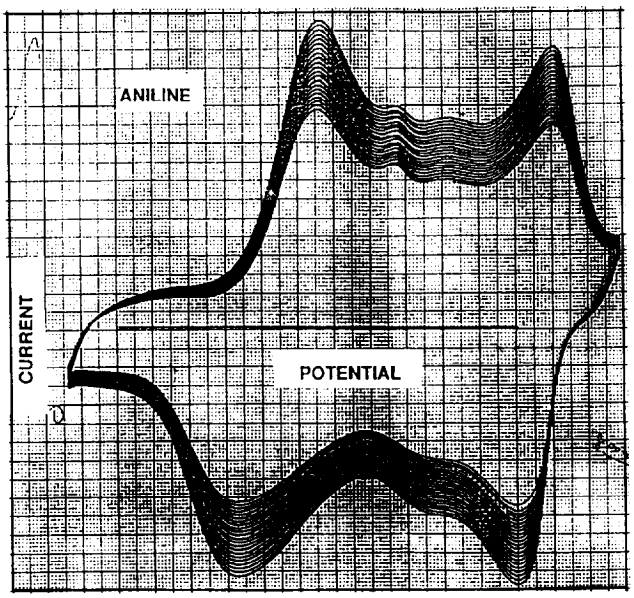

Fig. 16. 'Mirror-image' cyclic voltammograms corresponding to redox pseudocapacitance developed with a polyaniline film formed by potential cycling of an Au electrode in aq. aniline solution. Cyclic voltammograms for developed polyaniline film on Pt (Gu-Ping and Conway; cf. Ref. [16]).

from which C_{dl} could be evaluated if dV/dt at $t=0$ could be reliably evaluated. From an oscilloscope record, that derivative cannot be accurately determined by simply drawing a tangent to the rapidly declining $V(t)$ course at $t=0$, also where the IR drop fall of V can also usually be significant.

The following procedure can, however, be satisfactorily applied. The $V(t)$ transient is digitally recorded over 3–4 decades of t from μs to tens of ms and then curve-fitted by a suitable empirical function, e.g. $V(t)=a-bt\ \log(t+\tau)$ where a, b and τ are empirical constants. This function is then extrapolated to $t=0$, giving the potential $V(t=0)$ in the

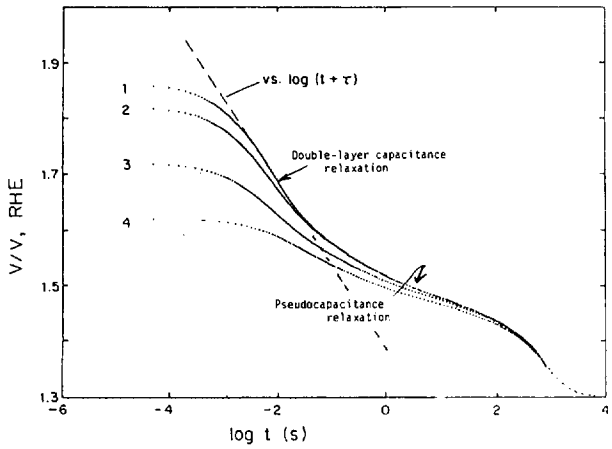

Fig. 17. Potential relaxation transients for O chemisorption at Pt from potentials of 1.88, 1.82, 1.71, 1.60 V RHE, showing distinction, in the time domain, between double-layer discharge and H pseudocapacitance relaxation processes. Potential relaxation of a previously polarized electrode after current interruption, on a log (t) plot (self-discharge of the double-layer capacitance plus any pseudocapacitance).

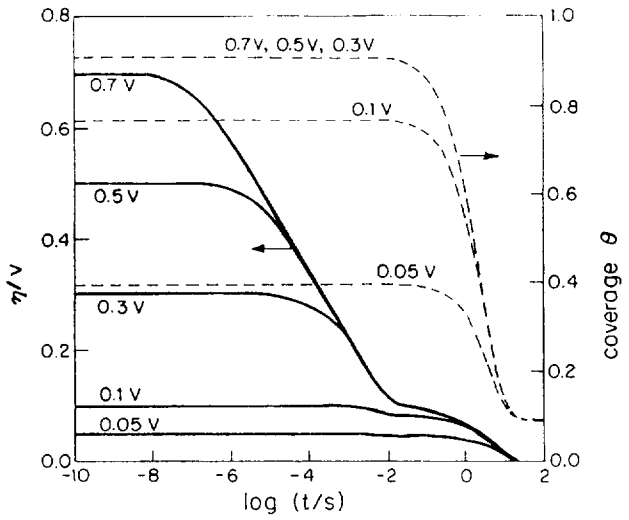

Fig. 18. Theoretical time dependence of potential in a relaxation transient and corresponding changes of coverage θ by an electrosorbed species. (In short-time range, no changes of θ arise, only double-layer discharge.) From Ref. [30].

absence of an iR drop, $V_{\text{initial}} - V(t=0) = iR$, is then obtainable. Correspondingly, $(dV/dt)_{t=0}$ is then calculated from the curve-fitted extrapolation function from which C_{dl} is then accurately obtainable without the uncertainty of geometrically attempting to draw tangents.

A procedure for analysis of whole time-domain transient curves, i.e. for $t>0$, $t \gg 0$, e.g. as shown in Fig. 17 which exhibits an arrest due to self-discharge of a pseudocapacitance, e.g. due to H chemisorption, was given by Harrigton and Conway [30]. The initial region of the transient was shown to be due almost entirely to relaxation of the double-layer charge (Fig. 18), corresponding limitingly ($t=0$) to Eq. (15), while the second arrest region is associated with self-discharge relaxation of the pseudocapacitance at longer times in the transient. The two regions in this 'time-domain' plot correspond to the two regions that can be distinguished in such a case in a 'frequency-domain' impedance complex-plane plot, where separate semicircles in complex-plane plots can be resolved for the double-layer and pseudocapacitance charge/discharge processes, as explained earlier.

Also in Fig. 18 is shown how the coverage θ of the electro-active species, e.g. H on the electrode surface, varies with time (and potential) in the $V(t)$ transient: only over the longer time range of the time-domain plot is the C_ϕ component relaxed by desorption of the H by the coupled processes:

$$SH + H_2 + e^- \rightarrow S + H_2 + OH^- \quad (16)$$

$$SH + OH^- \rightarrow S + H_2O + e^- \quad (17)$$

which is equivalent to electrochemical recombinative desorption of 2H to H_2. Contrarily, discharge of C_{dl} proceeds by continuation of the initial Faradaic process: $e^- + S + H_2O \rightarrow SH + OH^-$, until the potential range of the above coupled desorption processes is reached in the $V(t)$ transient. Initially then

$$-C_{dl}(dV/dt) = i_0 \exp(-\alpha\eta F/RT) \quad (18)$$

the r.h.s. being the Tafel function for the polarization process at the moment of current interruption, $t = 0$.

The pseudocapacitance, C_ϕ, as a function of potential, and the potential dependence of the coverage (here θ_H) of the electro-active species, H at Pt, giving rise to the C_ϕ, can be derived from the rate-constant parameters determined by a kinetic simulation treatment of the $V(t)$ transient in a way analogous to that applied to the corresponding frequency-response spectrum revealed by a.c. impedance.

References

[1] *Encyclopædia Britannica*, Vol. 6, COLE to DAMA, 14th edn., 1926, New York, p. 216.
[2] H.E. Becker (General Electric), *US Patent No. 2 800 616* (1957).
[3] I.D. Raistick and R.A. Huggins, *Mater. Res Bul., 18* (1983) 337.
[4] I.E. Raistrick, in J. Mattardy and F. Ludwig (eds.) *Electrochemistry of Semiconductors and Electronics*, Noyes, Park Ridge, NJ, 1992, Ch. 7.
[5] B.E. Conway, *J. Electrochem. Soc., 138* (1991) 1539.
[6] B.E. Conway and D. Craig, Rep. to Continental Group Inc., No. 1, 1975, Ref. 5.
[7] D.C. Grahame, *Chem. Rev., 47* (1947) 441
[8] R. Parsons, *Mod. Asp. Electrochem., 1* (1954) Ch. 2; J.O'M. Bockris, B.E. Conway and E. Yeager, *Comprehensive Treatise of Electrochemistry*, Vol. 1, Plenum, New York, 1981, p. 1.
[9] M. Born, *Z. Phys., 1* (1920) 45.
[10] B.E. Conway, *Ionic Hydration in Chemistry and Biophysics*, Elsevier, Amsterdam, 1981, Ch. 15.
[11] A. von Helmholtz, *Wied. Ann., 7* (1879) 337.
[12] G. Gouy, *Ann. Phys. (Paris), 7* (1917) 183
[13] O. Stern, *Z. Elektrochem., 30* (1924) 508.
[14] J.C. Currie, in M. Tomkiewicz and P.N. Sen (eds.) *Chemistry and Physics of Composite Media*, Vol. 85-8, The Electrochemical Society, Pennington, NJ, USA, 1985 p. 174; J.C. Currie (Sohio), *US Patent No. 4 730 239* (1988).
[15] K. Kinoshita, *Carbon*, Wiley, New York, 1980, pp. 441–532.

[16] A.F. Burke, Testing of ultracapacitors for electric vehicle applications, in S.P. Wolsky and N. Marincic (eds.) *Proc. 3rd Int. Seminar Double Layer Capacitors, Deerfield Beach, FL, USA, 1993*, Boca Raton, FL, 1993, Paper No. 2.
[17] J.W. Schultze and E. Koppitz, *Electrochim. Acta, 21* (1976) 327.
[18] J.W. Schultze and E. Koppitz, *Electrochim. Acta, 21* (1976) 337.
[19] P. Delahay, *J. Electroanal. Chem., 16* (1968) 131; *J. Phys. Chem., 70* (1966) 2373; *71* (1967) 3360.
[20] W. Lorenz and G. Salié, *Ber. Bunsenges. Phys. Chem., 69* (1964) 197.
[21] R. Haering and R. MacKinnon, *Mod. Asp. Electrochem., 15* (1983) 154.
[22] J. Thompson, *J. Electrochem. Soc., 126* (1979) 608.
[23] B.E. Conway and E. Gileadi, *Trans. Faraday Soc., 58*, (1962) 2493.
[24] A. Rudge and S. Gottesfeld, *J. Power Sources, 47* (1994) 89.
[25] F.G. Will and C.A. Knorr, *Z. Elektrochem., 64* (1960) 258.
[26] K. Engelsman, W.J. Lorenz and E. Schmidt, *J. Electroanal. Chem., 114* (1980) 1.
[27] S. Srinivasan and E. Gileadi, *Electrochim. Acta, 11* (1966) 321.
[28] H.A. Kozlowska, B.E. Conway and J. Klinger, *J. Electroanal. Chem., 75* (1977) 45.
[29] S. Hadzi-Jordanov, H.A. Kozlowska and B.E. Conway, *J. Electrochem. Soc., 125* (1978) 1471.
[30] D. Harrington and B.E. Conway, *J. Electroanal. Chem., 189* (1989) 1.
[31] L. Bai and B.E. Conway, J. R. S. Chem., *Faraday Trans., 63* (1993) 241.